

**LIG: a miniature 10 pm accuracy
Laser Interferometer Gauge**

Report of work performed under ESA contract
ITI 4000116275/16/NL/MH/GM

Written by

Anna M. Nobili, Marco Pisani & Massimo Zucco

March 2017; Final revision 5 May 2017

Contents

1	The goals of LIG within ESA contract ITI 4000116275/16/NL/MH/GM and structure of this report	3
2	Premise and motivations	4
2.1	Accelerometers in space	4
2.2	Capacitance readout vs heterodyne laser interferometer readout	6
2.3	ONERA capacitance sensors	7
2.4	Capacitance sensors of LISA-PF	8
3	LIG heterodyne interferometer	10
3.1	The breadboard	10
3.2	Measured displacement noise	14
3.3	Measured laser frequency noise	15
4	Comparison with other interferometers	17
5	Conclusions and prospects for the future	19
6	References	21

1 The goals of LIG within ESA contract ITI 4000116275/16/NL/MH/GM and structure of this report

The LIG (“Laser Interferometry Gauge”) proposal submitted to ESA in order to develop a readout based on laser interferometry capable of replacing with a better performance, as well as effectively (in terms of implementation onboard of a spacecraft) the capacitive readout currently used in most space accelerometers.

The specific contract no. 4000116275/16/NL/MH/GM was granted by ESA within the ITI (“Innovation Triangle Initiative”) program with the following goals:

- Realize a laser gauge with a displacement noise of $10 \frac{\text{pm}}{\sqrt{\text{Hz}}}$ at 1 Hz
- Provide a compact breadboard of the laser gauge
- Discuss realistic prospects for :
 - (i) achieving a displacement noise of $1 \frac{\text{pm}}{\sqrt{\text{Hz}}}$ at 1 Hz
 - (ii) reducing noise at low frequencies $1 \text{ mHz} \leq \nu < 1 \text{ Hz}$

This document reports on the achievement of the goals listed above (even better than planned) and is organized in accordance with the WBS (Work Breakdown Structure) of the proposal as follows.

WP#1 (LIG proposal management) was carried out by the University of Pisa. It covered the organization of the various phases of the research activity, the procurement of all necessary items, the distributions of work loads. It was organized through weekly teleconferences and written minutes, if needed, of issues covered and actions to be carried out in order to cover all work packages as planned in the original proposal and agreed at the time of contract kick-off.

In Sec. 2, which covers work package WP#2, we present a theoretical analysis and state of the art on accelerometers in space and discuss the advantages of laser interferometry versus capacitive readout.

In Sec. 3 we present the LIG setup and breadboard (Sec. 3.1, covering WP#3) and the experimental results in terms of displacement noise (Sec. 3.2) and laser frequency noise (Sec. 3.3), covering WP#4. In Sec. 4 we complete the analysis of our experimental results by comparing them with those of other laser interferometers.

Finally, in Sec. 5 we report on WP#5 by showing how to proceed in order to further improve the original goals of the contract and the results achieved so far.

2 Premise and motivations

2.1 Accelerometers in space

Accelerometers have been used in space soon after the start of the space age.

Measurement of the gravitational field of the Earth (space geodesy) requires to measure non gravitational accelerations (due to air drag, solar radiation pressure, non-isotropic thermal emission etc...) for them to be either separated out *a posteriori* or compensated by drag-free control.

The same need arises in exploring the solar system, when the motion of space probes in the gravitational field of celestial bodies other than Earth provides their knowledge only to the extent that non gravitational accelerations are measured.

Fundamental physics experiments in space are very often based on the measurement of very small gravitational accelerations, which again requires any spurious acceleration of the test (proof) mass relative to the spacecraft to be measured.

Accelerations of interest are low, below 1 Hz, while sonic vibration noise of spacecraft structures occurs at much higher frequencies and does not compete with them (see e.g. [1]).

Accelerometers are required to measure accelerations (in fact, relative accelerations).

They do that by measuring over the time the relative displacements of a test mass relative to the spacecraft structure to which it is weakly coupled, either mechanically or electrostatically inside an appropriate cage (as rigid and thermally stable as possible).

Once the nature of the coupling has been characterized (by means of the transfer function, obtained by theoretical analysis, numerical simulations and direct appropriate experimental measurements – e.g. of the quality factor of the coupling), the measured relative displacements of the test mass relative to the s/c provide their relative acceleration.

From a very general point of view, accelerations acting on the test mass can be divided in two, conceptually very different, types based on their different physical nature,

One type is an inertial acceleration, equal and opposite to that of any non gravitational acceleration acting on the s/c structure and not on the test mass inside it. This occurs in any accelerated, hence non inertial reference frame (the s/c), whereby complicated effects on the s/c structure produce the same effect on any test mass inside it, independently of its mass and composition because of the equivalence between inertial and gravitational mass. What makes the difference is only the coupling of the test mass to the s/c: test masses with (ideally) the same coupling would measure the same inertial acceleration. Inertial accelerations of a test mass can be used as input signal inside a drag-free control loop to make the s/c follow (by means of thrusters as actuators) the motion of the test mass.

The second type of accelerations on the test mass come from non gravita-

tional forces arising inside the cage enclosing it and not due to effects on the outer surface of the s/c or its structure. A well known example is the radiometer effect: residual air pressure inside the cage combined with a temperature gradient across the test mass does give rise to an acceleration relative to the cage. Unlike the inertial accelerations discussed earlier, the acceleration caused by direct non gravitational forces arising inside the cage depend on the specific test body used, typically on its mass and shape through the area-to-mass ratio. These are non-gravitational accelerations acting directly on the test mass.

As long as such non-gravitational accelerations are lower than the inertial ones, accelerometers can be regarded as inertial sensors and can be used to effectively drive a drag-free control loop so that the resulting motion of the s/c is governed only by the gravitational forces of interest.

Finally, it is worth recalling that if a test mass is not located exactly at the center of mass of the spacecraft, it will be subjected to gravity gradient (tidal) accelerations in the field of the primary body (e.g. the Earth). Being of gravitational nature, tidal accelerations cannot be distinguished (because of the equivalence principle) from the inertial ones. Of course, they must not be used to drive the drag-free control loop. Instead, they must be identified based on their specific signature, known from celestial mechanics, and from measurement of the offset relative to the center of mass of the s/c.

Any local unbalanced mass would also produce a tidal effect on the test mass which, if changing with time (e.g. because of thermal expansion/contraction) should be identified and modelled.

Last but not the least, since the gravitational accelerations of interest are small, any electric charge effect on the test mass would be disastrous. In space electric charging certainly occurs because of cosmic rays, making electric discharging of the test mass a crucial issue. The simplest and least expensive way to achieve that is by passive electric grounding through a mechanical connection between the test mass and its cage (as in the French accelerometers by ONERA and in the Italian ISA accelerometers). Active discharging, obviously of higher cost and complexity (as in GPB and LISA-PF), has also been demonstrated. Despite electric grounding or electric discharging, patches of electric charges are known to be present on the surfaces of conductors. Their effect proved to be very dangerous in the GPB mission devoted to the measurement of the Lense-Thirring effect, making them a relevant issue ever since.

Any given accelerometer relies, in order to provide a measurement of the acceleration of its test mass relative to the s/c, to read the relative displacements between the test mass and its cage. The lower the noise of the displacement readout, the better the measurement of the acceleration.

We show that a displacement readout based on heterodyne laser interferometry is the best solution for the accelerometers of interest in space described above.

2.2 Capacitance readout vs heterodyne laser interferometer readout

Space accelerometers based on capacitance readout rely on the fact that as the test mass moves relative to its cage, the separation between electrodes facing each other on the two objects changes, and so does the capacitance.

Since the capacitance is inversely proportional to the mutual separation D of the facing surfaces, the sensitivity of capacitance sensors is $\propto \frac{1}{D}$, hence the need of very small gaps. However, small gaps also mean that disturbing spurious effects such as residual gas damping and electric patches are larger, possibly impairing the measurement of the small effects of interest.

In order to provide a displacement, capacitance sensors must be calibrated so as to establish experimentally the factor between the voltage measured (in V) and the displacement (in m) which caused it. Capacitance sensors are analog sensors. If a displacement between zero and 1 cm yields a signal between zero and 1 V, a 1 pm displacement means a signal $\Delta V = 10^{-10}$ V, hence a very demanding signal-to-noise ratio (SNR) of 10^{10} .

Laser interferometers measure displacements in terms of the wavelength λ of the laser; therefore, they are linear with the displacement and are not limited by the size of the gap. The wavelength of the laser is very well measured, hence calibration is not required.

Laser interferometry sensors are partially digital (for displacements $> \lambda$) and partially analog (for displacements $< \lambda$). In the same example reported above, detecting 1 pm between zero and 1 cm with a laser of wavelength $\lambda \simeq 1 \mu\text{m}$ means a displacement signal $10^{-6} \lambda$, hence a SNR of 10^6 , which is 10^4 times less demanding than it is for capacitance sensors.

Laser heterodyne interferometers have the additional advantage that the signal is AC (at the heterodyne frequency ν_{het}), hence also immune to DC light. They measure the displacement as a phase difference (as in the case of LIG; see Sec. 3.2), or a time delay. For instance, with $\nu_{het} = 10$ kHz, if the time delay is measured with a high speed clock (at 500 MHz), the signal is digitized to $\lambda/50000 \simeq 0.02$ nm (for $\lambda \simeq 1 \mu\text{m}$), which is very good. Cap sensors also have an AC pumping voltage at e.g. 100 kHz, but no such advantage as in digitization of the signal, and in not needing calibration

2.3 ONERA capacitance sensors

The best results with capacitance sensors have been achieved by ONERA, a French Institution active in this field since several decades.

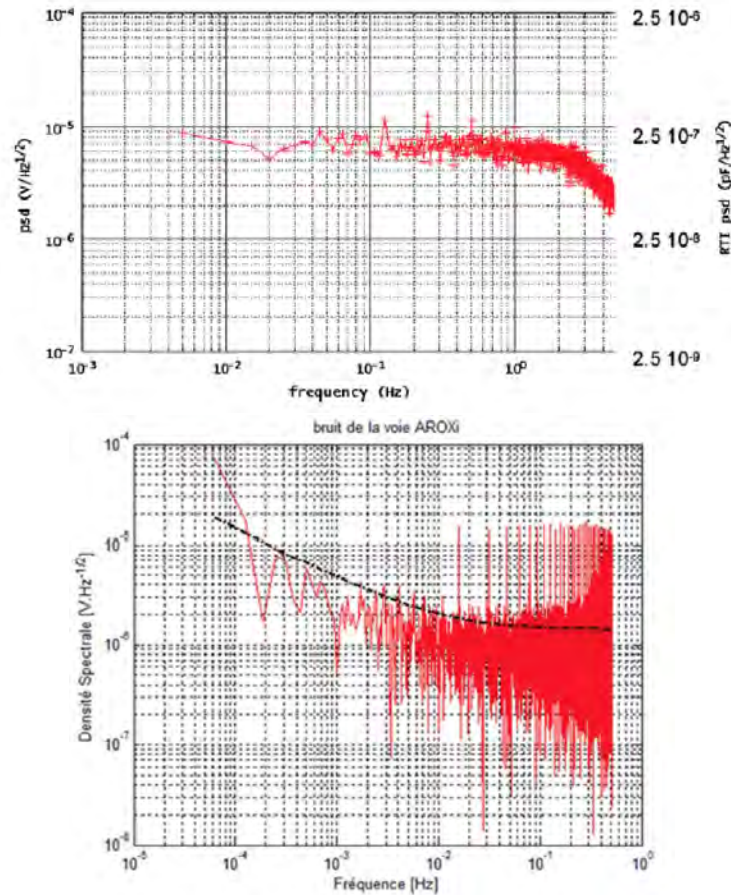


Figure 1: Noise spectrum of the Microscope accelerometer ($600\ \mu\text{m}$ gap) as reported in 2009 (top plot; see [2, 3]) and in 2013 (bottom plot; the black curve gives the required noise; see [4]). In [3] the calibration given was $6\ \mu\text{m}$ for $1\ \text{V}$. With this number the horizontal line at $10^{-5}\ \text{V}/\sqrt{\text{Hz}}$ corresponds to $60\ \text{pm}/\sqrt{\text{Hz}}$.

The most recent capacitance accelerometer by ONERA is currently flying on the Microscope satellite, launched on 25 April 2016 with the aim of testing the Weak Equivalence Principle to 10^{-15} .

The gap between the test mass and the cage is $600\ \mu\text{m}$ and there is a thin gold wire connecting the two which provides, in particular, electric grounding.

The electronic noise of the Microscope sensor prior to its launch (as of 2009 [2, 3] and 2013 [4]) is reported in Figure 1, expressed in $\text{V}/\sqrt{\text{Hz}}$ and/or $\text{pF}/\sqrt{\text{Hz}}$.

With the calibration provided, $1\ \text{V}$ (corresponding to $2.5 \cdot 10^{-2}\ \text{pF}/\sqrt{\text{Hz}}$) amounts to $6\ \mu\text{m}$ displacement. We therefore read $40\ \text{pm}/\sqrt{\text{Hz}}$ in the top graph

while in the lower one it is smaller between 1 mHz and 10 mHz (not exceeding about $20 \text{ pm}/\sqrt{\text{Hz}}$), increasing at lower frequencies to exceed $40 \text{ pm}/\sqrt{\text{Hz}}$.

A comprehensive theoretical analysis was published in 1999 by the French scientists[5], including also a graph of the measured noise (with appropriate calibration) that we report in Figure 2. The gap in this case was $300 \mu\text{m}$, half that of the microscope accelerometer. As the figure shows, above 0.01 Hz noise is $22 \text{ pm}/\sqrt{\text{Hz}}$ (flat), while at $\nu \lesssim 0.01 \text{ Hz}$ it grows up to $200 \text{ pm}/\sqrt{\text{Hz}}$ (and more) below mHz.

It seems very hard to push the noise of capacitance sensors below 10 or even $20 \text{ pm}/\sqrt{\text{Hz}}$, and $1/f$ growth at low frequencies is always there. In addition, there is no way to avoid very small gaps.

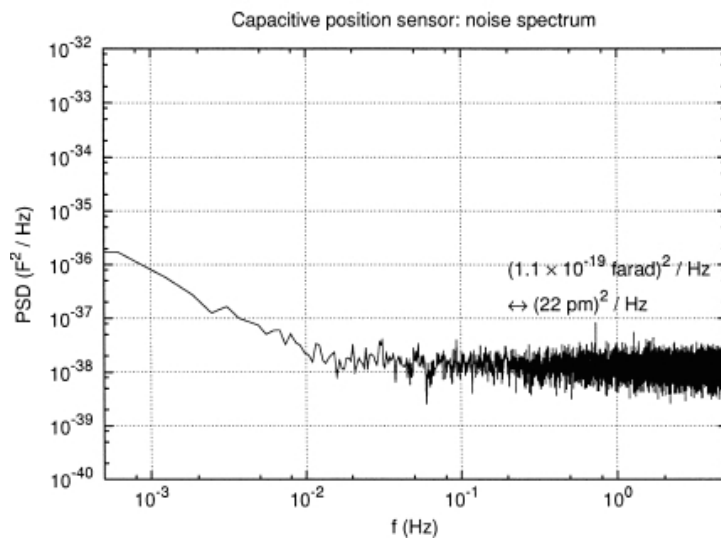


Figure 2: Noise spectrum of the capacitance position sensor by ONERA, with $300 \mu\text{m}$ gap, as published in 1999[5]. At $\nu \gtrsim 0.01 \text{ Hz}$ noise is $22 \text{ pm}/\sqrt{\text{Hz}}$ flat. The knee at 0.01 Hz and noise growth below this frequency is attributed by the authors to the low frequency amplifier. The largest value shown in this plot amounts to about $280 \text{ pm}/\sqrt{\text{Hz}}$.

2.4 Capacitance sensors of LISA-PF

LISA-PF has recently flown two accelerometers[6] whose test masses (of cubic shape, 2 kg each) are located 38 cm apart, each one inside its own cage with 4 mm gap and no physical contact with it, the suspension being provided by electrostatic forces. They mimic the two mirrors of the gravitational wave antenna which in the real LISA mission will be placed inside two different spacecraft separated by $5 \cdot 10^6 \text{ km}$.

In this case the requirement on the capacitance readout noise is of several $\text{nm}/\sqrt{\text{Hz}}$ at mHz, much higher than in Microscope (see Figure 3). It is auxiliary to a more precise readout provided by laser interferometry (see Sec. 4).

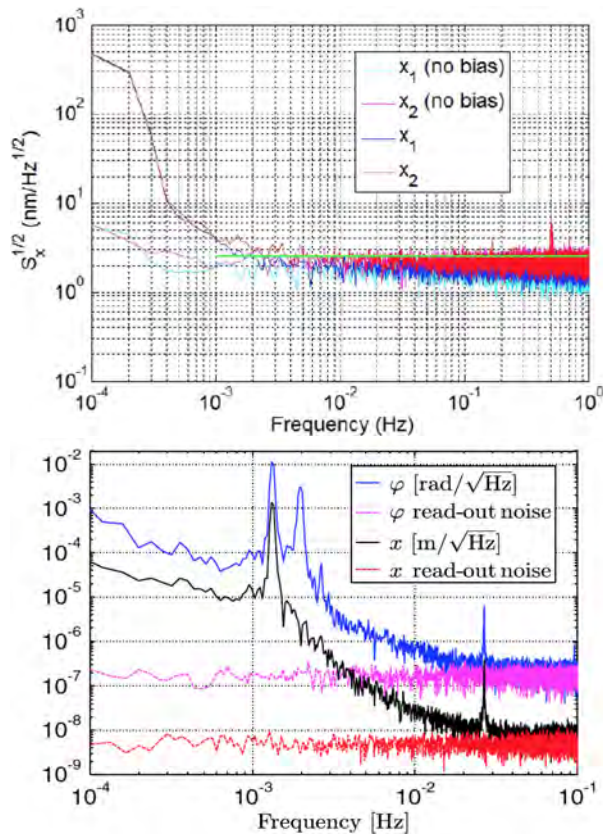


Figure 3: Noise spectrum of LISA-PF capacitance readout: (*top*) as reported in 2010 at the 8th LISA Symposium[7] and (*bottom, red curve*) as measured with a double torsion pendulum in 2016[8].

The drag-free control loop, closed on one test mass, is driven by the laser readout which reads also the motion of the second test mass relative to it and drives the capacitors as actuators for the second mass to follow the first one.

Being located in the L1 point, at about 1.5 million km from Earth, the effect of residual air drag on LISA-PF is much smaller than it is on satellites in low Earth orbit such as Microscope (at 700 km altitude). However, solar radiation pressure cannot be avoided and turns out to be only about 4 times smaller than air drag at 600-700 km. While in the real LISA experiment the test masses will be located inside two different spacecraft several million km apart, in LISA-PF they are both inside the same spacecraft, at 38 cm distance. Hence, the resulting inertial acceleration on the test masses is ideally the same (common mode) and can be partially removed (*a posteriori*, via software) from their relative motion, making their relative (non gravitational) acceleration very small. Thus –in the frequency range of interest– the relative motion of the test masses is (to the extent achieved) purely gravitational, and would therefore include the differential effect of a gravitational wave which is obviously negligible over 38 cm and could only be detected in the real LISA mission.

3 LIG heterodyne interferometer

In this section we describe the LIG heterodyne interferometer realized within the ITI contract. We report the noise spectrum of the measured displacement, the noise spectrum of the measured frequency of the laser, and finally compare our results with those of other laser interferometers.

3.1 The breadboard

The key components and characteristics of the LIG interferometer are the following:

- A polarization maintaining ORION RIO laser with $\lambda = 1064$ nm, 11 mW power of which about 1 mW used
- Two acousto-optic modulators AOMs at frequencies of 80 MHz and 80.1 MHz resulting in heterodyne frequency $\nu_{het} = 100$ kHz
- The laser is not locked for frequency stabilization (free-running laser)
- The measurements are performed in air; the optical head is mounted on a zerodur base and placed inside a box with foam in order to prevent turbulence

Figure 4 shows a sketch of the optoelectronic board and of the optical head.

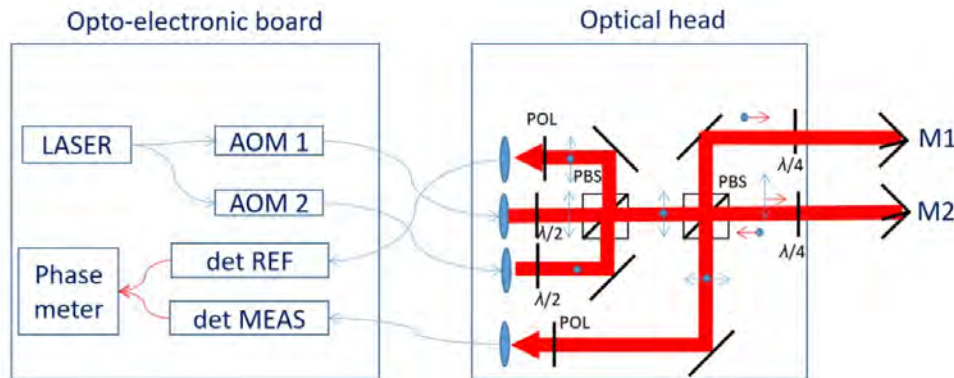


Figure 4: Sketch of the optoelectronic board and of the optical head of the LIG heterodyne interferometer.

A scheme of the interferometer is shown in Figure 5. The laser sources L1 and L2 emit two linearly polarized beams at frequency ν_1 and ν_2 with $\nu_1 - \nu_2$ the heterodyne frequency. A single laser source is split into two equal parts that are frequency shifted by means of acousto-optic modulators (AOM) at two slightly different frequencies and finally sent to the interferometer. Two half

wave plates (HWP) are used to correct the orientation of the polarization axes so that the two are mutually orthogonal. A polarizing beam splitter (PBS) combines the two beams into a single one. A Beam splitter (BS) reflects a portion of the two beams and sends them towards the detector D1. A polarizer at 45° selects a portion of the two orthogonally polarized beams in order to obtain the interference signal. This signal is the reference for the phase-meter. A second PBS separates the two beams and sends them respectively to the two mirrors M1 and M2. A quarter wave plate (QWP) placed in between the PBS and the mirror makes the polarization circular. When the circularly polarized beam is reflected by the mirror and passes through the QWP again, it is transformed into a linearly polarized beam orthogonal to the original one. This method allows the PBS to redirect the two reflected beams towards the detector D2. The interference signal generated here has a phase delay with respect to the reference signal, which is proportional to the optical path difference, in its turn proportional to the relative displacement of the two mirrors.

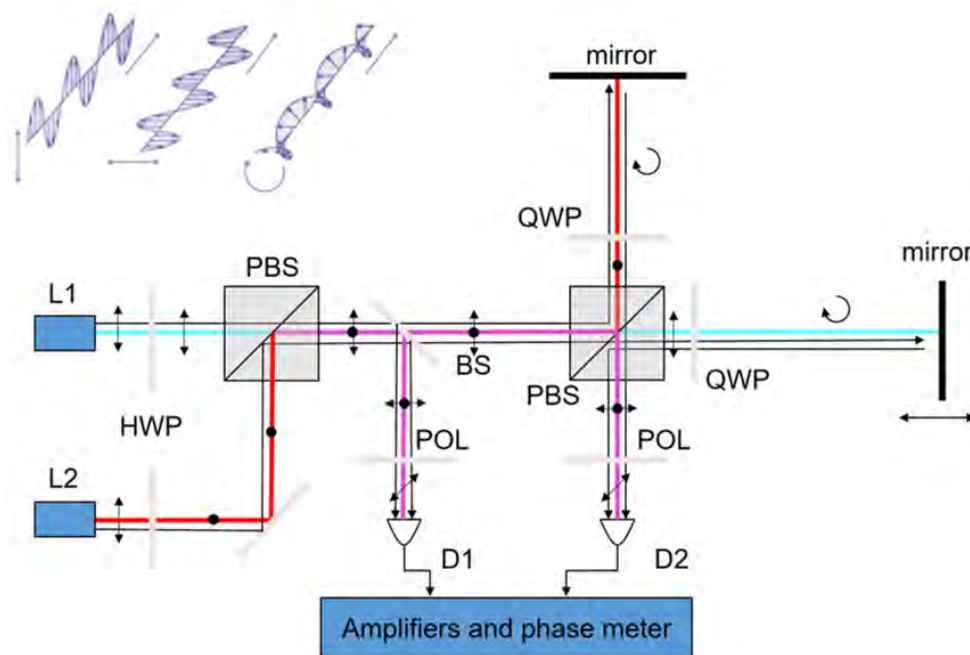


Figure 5: Detailed schematic of the LIG heterodyne interferometer. See text for its description.

A detailed diagram of the optoelectronic board is given in Figure 6 (top), while the bottom chart depicts all its components in 3D and how they are arranged on a 39 by 32 cm board. The total mass amounts to 2.35 kg with a total power consumption of about 40 W (using standard components not optimized for space).

A picture of the optical head is shown in Figure 7.

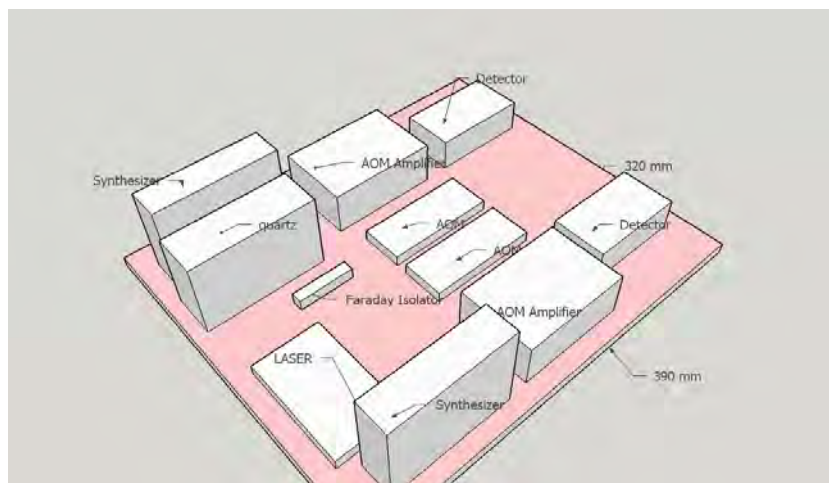
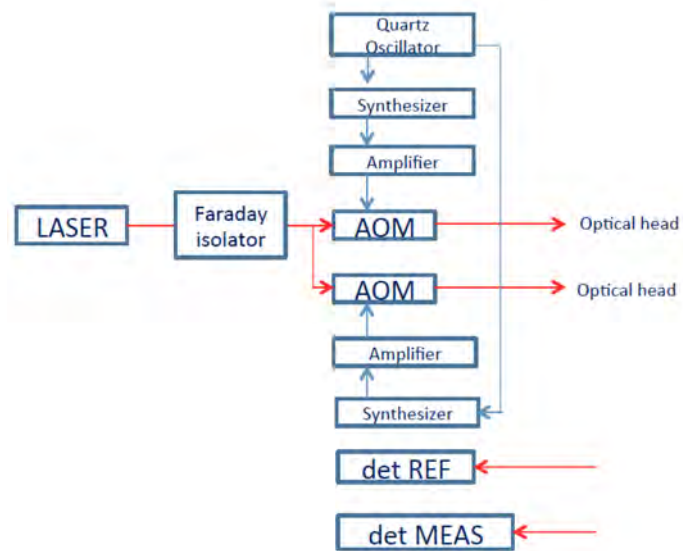


Figure 6: Top: diagram of all the components of the optoelectronic board. Bottom: 3D view of the same components in the way they are physically arranged. The overall dimensions are shown, the total mass is 2.35 kg and the total power is about 40 W (with ordinary components not optimized for use in space).

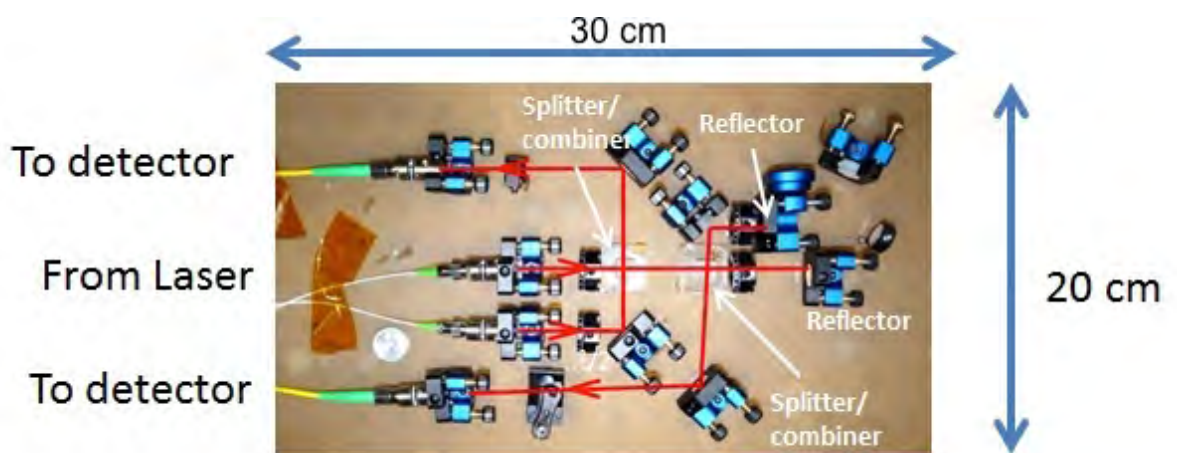


Figure 7: Picture of the optical head of LIG. It is mounted on a zerodur base and operated in air inside a box with foam. The size shown can ultimately be reduced to a chip with two fibers as input from the laser source and two as output toward the detectors. The total mass is about 0.5 kg.

3.2 Measured displacement noise

The signals generated on the detectors D1 and D2 shown in Figure 5 are amplified via low noise amplifiers, they are acquired at 400000 sample per second and 16 bit resolution and elaborated by a LabView based software. The software implements classical I/Q demodulation in order to extract the sine and cosine components of the phase vector. Finally, the phase is extracted 1000 times per second, converted into displacement and recorded. The very large number of data available ensures a very good signal-to-noise ratio.

The spectrum of the displacement noise measured with the setup presented in Sec. 3.1 is reported in Figure 8.

We notice the following:

- At 1 Hz the noise measured is $0.6 \frac{\text{pm}}{\sqrt{\text{Hz}}}$, which is better than the target set for the ITI contract by a factor 16.7
- At high frequencies the noise measured is about $0.1 \frac{\text{pm}}{\sqrt{\text{Hz}}}$ and it is identified as electronics noise, due to the ADC converter and digital demodulation (it is not interferometer noise).
- The increase of noise at $\nu < \text{Hz}$ down to 1 mHz (where it reaches about $1 \frac{\text{nm}}{\sqrt{\text{Hz}}}$) is rather peculiar. Our analysis shows that it is not due to air, neither to thermo-mechanical deformations nor to local terrain noise. We have clearly identified the optical fibers as responsible for it, and they are under investigation for LIG follow-up.

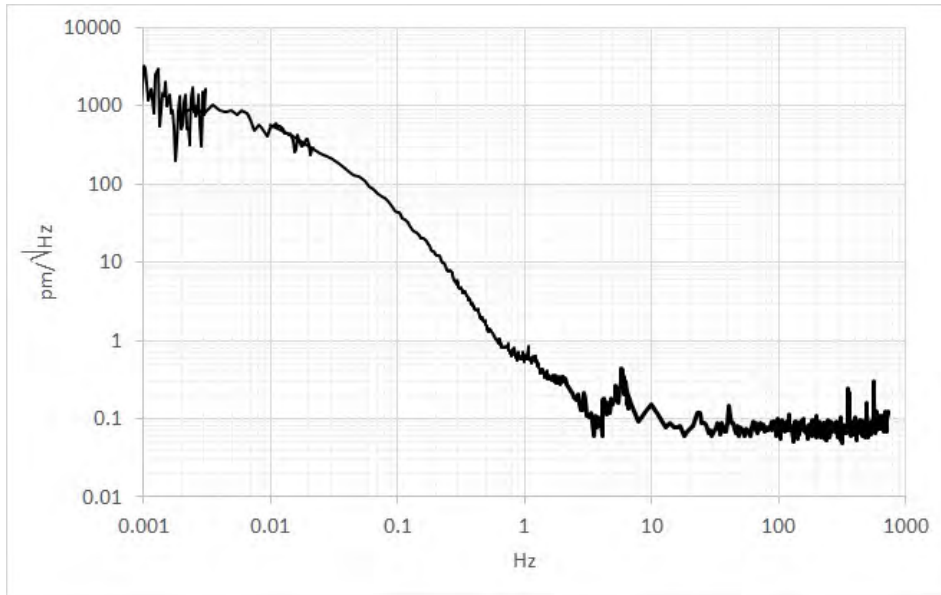


Figure 8: Noise spectrum of the displacement measured with LIG heterodyne interferometer described in Sec. 3.1.

3.3 Measured laser frequency noise

The displacement noise of the interferometer depends (particularly for large optical path differences) on the frequency noise of the laser.

A measurement of the frequency noise for the free-running diode laser RIO Orion with wavelength $\lambda = 1542$ nm was reported in [9], where the advantages of locking the frequency of the laser to acetylene have also been measured.

In Figure 9, taken from their work, we can see that at 1 Hz the frequency noise is slightly below 10^4 Hz/ $\sqrt{\text{Hz}}$ and its reduction in case of locking is by almost two orders of magnitude.

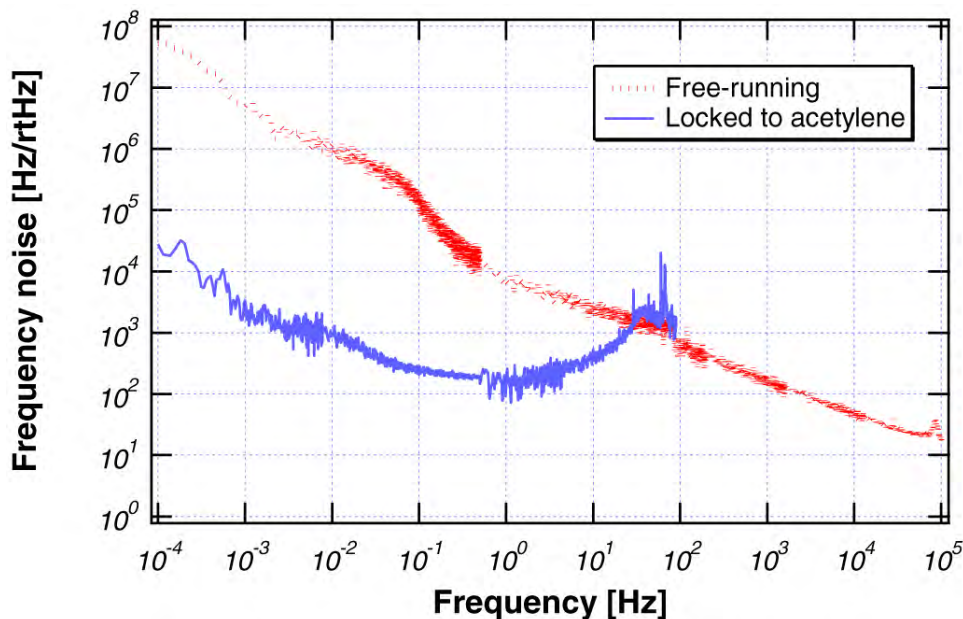


Figure 9: This figure (taken from [9]) shows the frequency noise as measured by the authors without (red curve) and with (blue curve) stabilization of the laser frequency.

The frequency noise can be obtained by measuring the frequency difference of two similar free-running lasers. However, the measurement of the frequency difference of two similar lasers may hide common mode effects –such as thermal drifts– which would obviously affect the measurement when using one individual laser. In order to make sure that the measured frequency noise of the free-running laser does not cancel any common mode noise we have measured the absolute frequency with the optical frequency comb of INRIM (the Italian Metrology Institute in Torino) directly traceable to the realization of the SI second, which measures the laser frequency with high accuracy. Our results are reported in Figure 10 and turn out to be comparable with those of Fig. 9 (red curve), thus confirming that this is the real long term frequency stability of the RIO Orion free-running laser. In particular at 1 Hz the frequency noise is 10^4 Hz/ $\sqrt{\text{Hz}}$, only slightly higher than the value measured by [9] and shown in Figure 9.

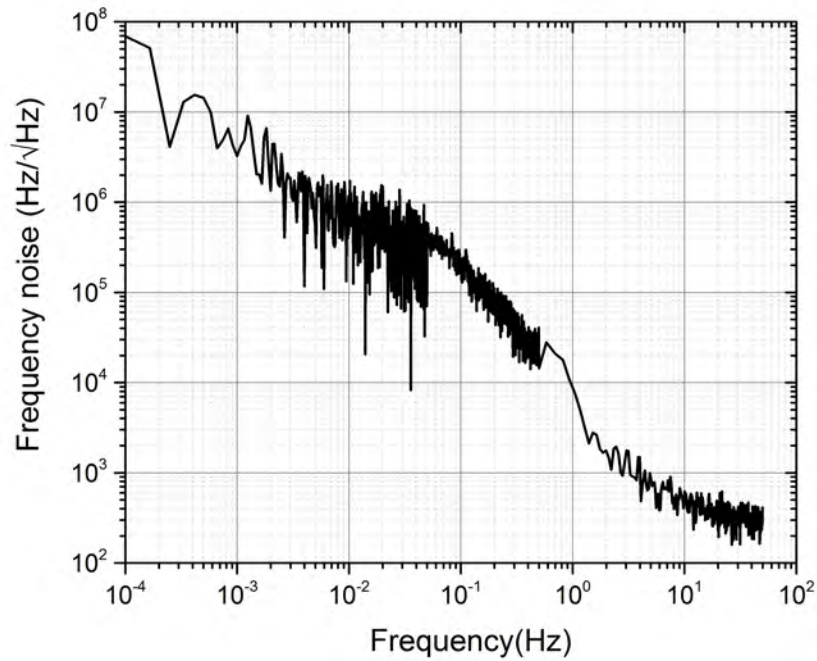


Figure 10: Power spectral density of the frequency fluctuations of the free-running diode laser RIO Orion at 1542 nm. It has been obtained by measuring the absolute frequency with the optical frequency comb of INRIM (the Italian National Metrology Institute in Torino) directly traceable to the realization of the SI second, so as not to be affected by common mode noise. It is comparable to the frequency noise measured by [9] and shown in Fig. 9 (red curve)

With this level of frequency noise, and for use with accelerometer gaps of the order of a cm, our results show no need to stabilize the frequency of the laser at 1 Hz. The issue needs to be further investigated at lower frequencies depending on the target noise.

4 Comparison with other interferometers

It is worth comparing the noise spectrum measured with LIG as reported in Sec. 3.2 with results obtained with other heterodyne laser interferometers.

The first comparison is with the laser gauge developed at JPL by Mike Shao for the SIM mission of NASA. Our work has indeed been stimulated by Mike Shao who pointed out to us the advantages of laser metrology over capacitance sensors as well as its feasibility[11].

The noise level achieved by the heterodyne laser gauge at JPL in the early 2000s is shown in Figure 11. It has reached $1 \text{ pm}/\sqrt{\text{Hz}}$ at 1 Hz; it is at about $0.4 \text{ pm}/\sqrt{\text{Hz}}$ at high frequencies; the increase at low frequencies is the measurement of a real thermal drift of the gauge head,

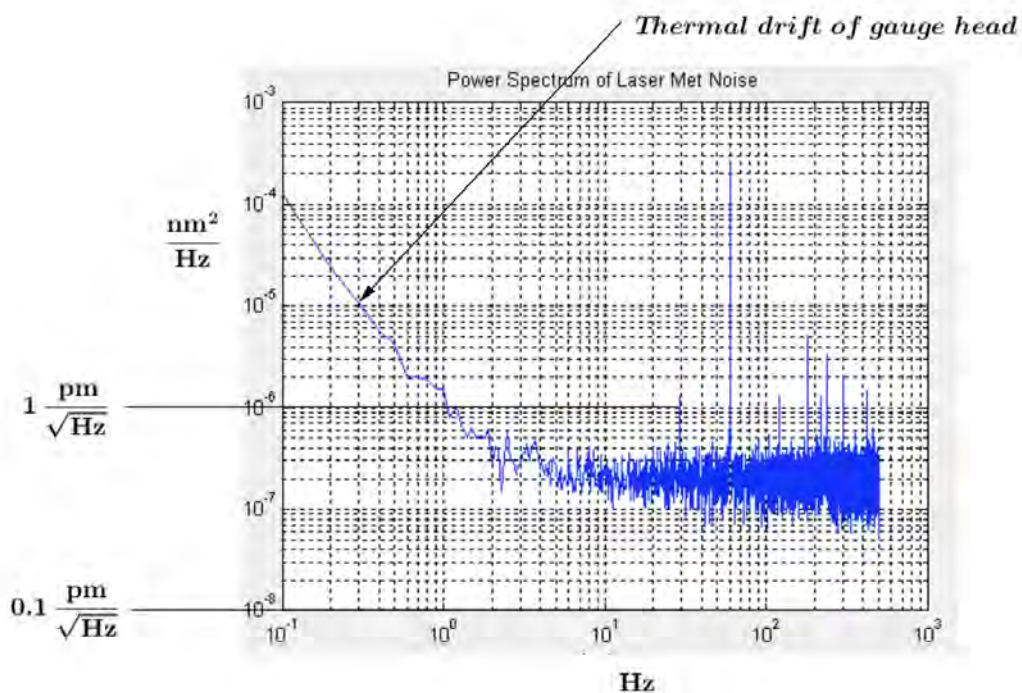


Figure 11: Noise spectrum of the laser gauge developed by Mike Shao at JPL in the early 2000s (kindly provided by the author).

LISA-PF has recently flown a heterodyne laser interferometer to measure the relative displacement of one test mass relative to the s/c (4 mm gap) and of the test masses relative to each other (38 cm apart). The frequencies of interest are between 1 mHz and 1 Hz. The frequency of the laser is stabilized and the length of optical fibers is actively controlled.

The spectrum of displacement noise as measured by LISA-PF on ground and in space is shown in Figure 12 and Figure 13 respectively.

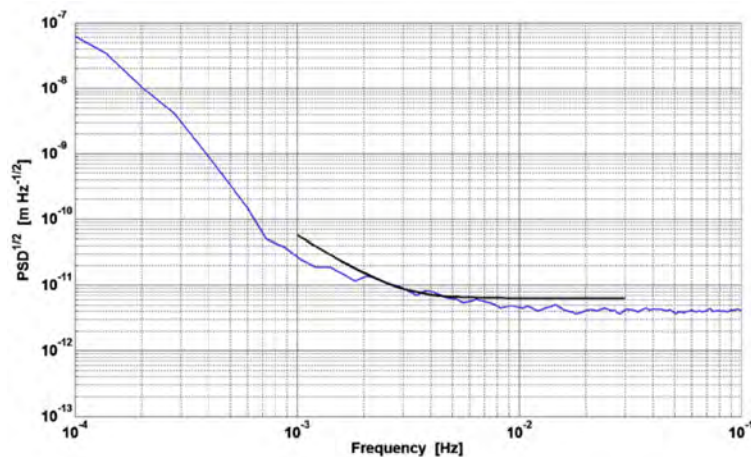


Figure 12: This plot is taken from [12] and shows the interferometer displacement noise required for LISA-PF (black curve, going from 6 to 60 pm/ $\sqrt{\text{Hz}}$) and the noise measured in the lab (blue curve, with a lowest level of 4 pm/ $\sqrt{\text{Hz}}$). Noise increase below 7 mHz is attributed by the authors to the laboratory environment.

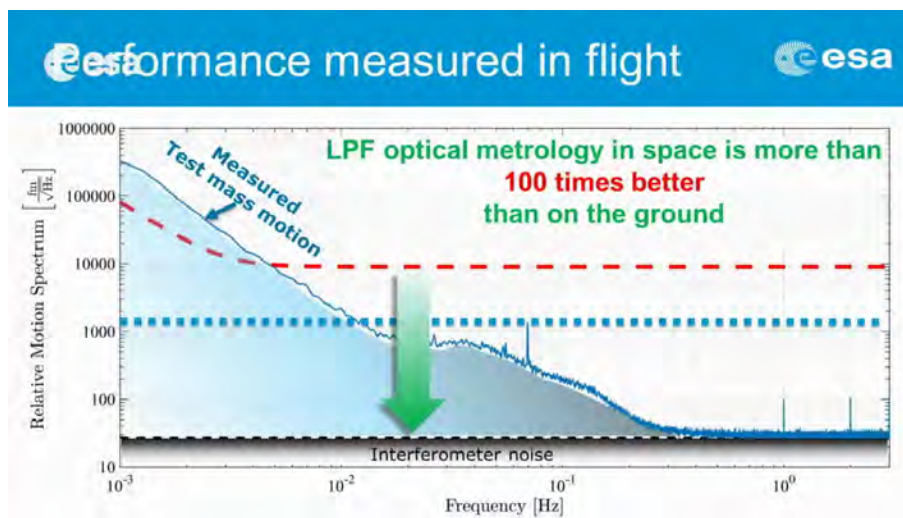


Figure 13: This plot was shown by Martin Hewitson during ESA press conference of 7 June 2016 in which the results of LISA-PF were presented. The lowest interferometer noise measured in space is about 2 orders of magnitude lower than on ground, reaching 0.03 pm/ $\sqrt{\text{Hz}}$, a factor of 3.3 better than measured by LIG (Figure 8). It is at this level also at 1 Hz, which is better than LIG by a factor of 20. Close to 1 mHz the noise currently reported with LIG in Figure 8 is 1 nm/ $\sqrt{\text{Hz}}$, only 3.3 times larger than reported here as measured by LISA-PF in space. Unlike in LIG, where it is a spurious effect due to the optical fibers, here it is a physical effect which must be subtracted (see [6]).

A different type of interferometer has been developed to read the motion of a test mass coupled to its cage (hence to the s/c) with very high stiffness, i.e. with very high resonance frequency (> 10 kHz); see [13].

A very high resonance frequency is convenient whenever the need is to measure high frequency effects. This is because in 1D oscillators forces acting above the resonance are attenuated (as the ratio applied-to-resonance frequency squared), making it easier to measure sub resonance effects. However, very high stiffness (i.e. very high resonance frequency) also mean very low sensitivity (the displacement produced on the test mass by a given acceleration scales as the inverse of its resonance frequency squared). As a result, if the test mass is characterized by very high resonance frequency, for it to be useful in measuring small accelerations the readout must have very low noise.

A laser interferometer based on a low finesse Fabry-Perot cavity with very small gap ($50 \mu\text{m}$) has been realized by [13], coupled with an oscillator with very high resonance frequency (10.65 kHz). Despite a displacement noise of only about $5 \text{ fm}/\sqrt{\text{Hz}}$ above a few kHz, the authors report that at 1 Hz it amounts to $2 \frac{\text{pm}}{\sqrt{\text{Hz}}}$, growing to $90 \frac{\text{pm}}{\sqrt{\text{Hz}}}$ at 0.01 Hz. More importantly, because of the low sensitivity, they result from accelerations as large as $8.8 \cdot 10^{-3} \frac{\text{ms}^{-2}}{\sqrt{\text{Hz}}}$ and $0.4 \frac{\text{ms}^{-2}}{\sqrt{\text{Hz}}}$ respectively.

It is apparent that this accelerometer and its laser readout are not suitable for the low frequency, small, effects of interest in space as discussed in Sec. 2.1 and addressed by the LIG heterodyne interferometer.

5 Conclusions and prospects for the future

In summary, the first two goals of the ITI contract recalled in Sec. 2 have been well achieved:

- The displacement noise measured at 1 Hz is smaller than the target by more than 1 order of magnitude.
- A compact breadboard of the LIG interferometer that has carried out the measurement is ready.

We also planned to investigate (within WP#5) realistic prospects for:

(i) achieving a displacement noise of $1 \frac{\text{pm}}{\sqrt{\text{Hz}}}$ at 1 Hz.

This is no longer an issue since we have already measured $0.6 \frac{\text{pm}}{\sqrt{\text{Hz}}}$ at 1 Hz (and $0.1 \frac{\text{pm}}{\sqrt{\text{Hz}}}$ above 10 Hz).

(ii) reducing noise at low frequencies $1 \text{ mHz} \leq \nu < 1 \text{ Hz}$.

We currently observe a noise increase below 1 Hz reaching about $1 \frac{\text{nm}}{\sqrt{\text{Hz}}}$ at 1 mHz. Specific checks have shown that it is due to the optical fibers. In fact, it has already been reduced to the level reported here by appropriately arranging them. Further reduction (for instance by ensuring that all components have the property of maintaining the polarization, that the length of the fibers and their connectors are suitable, by providing phase stabilization etc...) will be pursued in the LIG follow-up.

Finally, it is worth mentioning a very interesting new opportunity, although it was not planned when LIG was proposed and approved.

For a laser gauge such as LIG to be appreciated as an effective replacement of classical capacitive readout in accelerometers of interest in space we must demonstrate its performance in combination with an oscillator with reasonably low stiffness coupling, so that it is sensitive to the low frequency accelerations of interest.

We have such an oscillator. In a one-axis version its mass is about 700 g. Different designs of the oscillator can be envisaged, especially in absence of weight, with lower stiffness, hence with higher acceleration sensitivity for the same displacement noise of the laser interferometer readout. For demonstration of feasibility we need to implement the LIG readout so that it can provide the displacement of the test mass of the oscillator. The implementation requires the optical head of LIG (as described in Sec. 3.1, Fig. 7) weighing about 500 g in its current setup on a zerodur base, to be combined with the oscillator. As for the optoelectronic board, it will be the same as in Sec. 3.1, Fig. 6 –save for the modifications required to fix the low frequency noise due to the optical fibers– with the current mass of 2.35 kg and a power budget (not yet optimized for space) of about 40 W (as discussed in Sec. 3.1). Ultimately the optical head could be reduced to the size of a chip, with two fibers as input from the laser source and two as output toward the detectors, and its integration with the mechanical oscillator would be very compact indeed and competitive with capacitive accelerometers also in terms of complexity and costs.

On 16 February 2017 the ITI program was again open for applications, though not in the same form as before. It now refers to “Proof of Concept” proposals (as the LIG contract we are reporting about with this document) and “Demonstration of Feasibility & Use” proposals.

Building on what we have realized so far, a proposal of the latter kind –LIG-A: Laser Interferometry Gauge & Accelerometer– with the objective of setting up the breadboard of a sensitive laser read accelerometer, has been submitted.

References

- [1] A.M. Nobili *et al.*, Noise attenuators for gravity experiments in space, Phys. Lett. A 160, 45 (1991)
- [2] P. Touboul, The Microscope Mission and Its Uncertainty Analysis, Space Sci. rev. 148, 455 (2009)
- [3] M. Rodrigues, Development status of the Microscope payload, Talk given at “Gravitation and Fundamental Physics in Space”, Les Houches (2009)
- [4] M. Rodrigues, Microscope payload. Twin-Space Accelerometer for Gravitation Experiment T-SAGE, talk given at “Microscope second colloquium”, Paris (2013)
- [5] V. Josselin, P. Touboul and R. Kielbasa, Capacitive detection scheme for space accelerometers applications, Sensors and Actuators 78, 92 (1999)
- [6] M. Armano *et al.*, Sub-Femto-g Free Fall for Space-Based Gravitational Wave Observatories: LISA Pathfinder Results, Phys. Rev. Lett. 116, 231101 (2016)
- [7] W. J. Weber, Talk given at 8th LISA Symposium, Stanford (2010)
- [8] M. Bassan *et al.*, Approaching Free Fall on Two Degrees of Freedom: Simultaneous Measurement of Residual Force and Torque on a Double Torsion Pendulum, Phys. Rev. Lett. 116, 051104 (2016)
- [9] K. Numata, J. Camp, M. A. Krainak, and Lew Stolpner, Performance of planar-waveguide external cavity laser for precision measurements, Optics Express 18, 22781 (2010)
- [10] M. Pisani, M. Zucco, and A. M. Nobili, Laboratory tests of a high-precision laser interferometry readout for the GG experiment in space, IEEE 978-1-4673-8292-2/16, 260-265 (2016)
- [11] M. Shao, SIM metrology, Talk given at GG Workshop in Pisa (2010)
- [12] F. Antonucci *et al.*, From laboratory experiments to LISA Pathfinder: achieving LISA geodesic motion, Class. Quantum Grav. 28 (2011)
- [13] O. Gerberding *et al.*, Optomechanical reference accelerometer, Metrologia (2015) arXiv:1504.01055v1